

Tracking kidney stones in a homogeneous medium using a trilateration approach

Kya Shoar, Benjamin W. Turney, and Robin O. Cleveland

Citation: [The Journal of the Acoustical Society of America](#) **142**, 3715 (2017);

View online: <https://doi.org/10.1121/1.5017718>

View Table of Contents: <http://asa.scitation.org/toc/jas/142/6>

Published by the [Acoustical Society of America](#)

Articles you may be interested in

[Limitations on estimation of effective scatterer diameters](#)

The Journal of the Acoustical Society of America **142**, 3677 (2017); 10.1121/1.5017602

[Enhancing acoustic signal response and absorption of an underwater coated plate by embedding periodical inhomogeneities](#)

The Journal of the Acoustical Society of America **142**, 3722 (2017); 10.1121/1.5017604

[Elastic feature of cylindrical shells extraction in time-frequency domain using biomimetic dolphin click](#)

The Journal of the Acoustical Society of America **142**, 3787 (2017); 10.1121/1.5017835

[Pressure and tension waves from bubble collapse near a solid boundary: A numerical approach](#)

The Journal of the Acoustical Society of America **142**, 3649 (2017); 10.1121/1.5017619

[Coupled finite element/boundary element formulation for scattering from axially-symmetric objects in three dimensions](#)

The Journal of the Acoustical Society of America **142**, 3637 (2017); 10.1121/1.5016030

[Characterization of interface reflection coefficients using a finite-difference injection technique](#)

The Journal of the Acoustical Society of America **142**, EL579 (2017); 10.1121/1.5016467

Tracking kidney stones in a homogeneous medium using a trilateration approach

Kya Shoar,¹ Benjamin W. Turney,² and Robin O. Cleveland^{1,a)}

¹*Institute of Biomedical Engineering, Department of Engineering Science, University of Oxford, Oxford OX3 7DQ, United Kingdom*

²*Nuffield Department of Surgical Sciences, University of Oxford, Oxford OX3 9DU, United Kingdom*

(Received 13 August 2017; revised 19 November 2017; accepted 26 November 2017; published online 20 December 2017)

Shock wave lithotripsy is a non-invasive procedure by which kidney stones are fragmented by thousands of shock waves. Currently, many shock waves are delivered to the body that do not impact the stone, but do result in tissue trauma. This motivates developing a monitoring system to locate kidney stones, with the goal of gating shock waves not aligned with the stone, and hence, reducing renal trauma during lithotripsy. The system consists of a circular array housing twenty-two 0.5 MHz transducers that can be mounted on a clinical lithotripter. It was deployed in a water tank and tested with two stone models made from gypsum cement and a stone model fragment. An algorithm consisting of threshold detection, automatic rejection of weak signals, and triangulation was developed to determine the location of stones. The results show that within ± 15 mm of the focus of the lithotripter, the accuracy was better than 4 mm in the lateral directions and 2 mm in the axial direction. Using off-the-shelf hardware, the algorithm can calculate stone positions every 1 s allowing for real-time tracking during lithotripsy. © 2017 Acoustical Society of America.

<https://doi.org/10.1121/1.5017718>

[CCC]

Pages: 3715–3721

I. INTRODUCTION

Shock wave lithotripsy (SWL) is a non-invasive modality to treat kidney stones by fragmenting them into pieces small enough to pass naturally.¹ The procedure is generally considered safe, but concerns about renal injury due to SWL have been raised since the late 1980s.² Studies have shown acute effects such as hematuria, subcapsular hematomas,^{3,4} and in rare cases renal failure.^{5,6} Chronic effects, such as a new onset hypertension and recurring stone disease, have been suggested by some studies^{7,8} although there is not general acceptance. Studies in animals and patients indicate that adverse bioeffects in the kidney increase with the number of shock waves (SW) delivered,^{9–11} the rate of SW delivery,^{12,13} and the SW energy levels.¹⁴ If the number of SWs could be reduced without affecting outcomes, the risk of injury to the kidney should therefore decrease.

Stone motion, due to respiration and/or patient motion during the procedure, means that as few 40% of the SWs delivered to the body hit their target due to misalignment of the SW focus and the kidney stone.¹⁵ The mistargeted SWs will therefore induce tissue damage without providing a therapeutic effect. Hence, it follows that if the stone can be tracked in real-time, the delivery of SWs can be gated to ensure that SWs are only fired when the stone is in the focus, and the number of SWs reduced. Such systems have been proposed in the past. For example, Orkisz *et al.* used B-mode ultrasound and a block matching algorithm to determine the location of kidney stones in real-time and showed 40% fewer shocks were necessary to fragment kidney stones

through tracking.^{16,17} Similarly, Chang *et al.* designed an algorithm to compute stone trajectories from B-mode imaging in patients.¹⁸ The trajectories were used in *ex vivo* and *in vitro* models to move stones using a computerised positioning stage,¹⁹ and by tracking the stone during lithotripsy, the number of SWs was reduced by half. Furthermore, all of the tracked stones were pulverised to less than 1 mm compared to 55.3% for untracked stones. Such algorithms demonstrate the utility of tracking, but they rely on B-mode ultrasound imaging, which is not a robust method of finding stones, for example, sensitivity values range from 19% to 93% and specificity values from 84% to 100% for detecting stones using B-mode ultrasound.²⁰ It appears that reliance on B-mode has been a barrier to clinical translation.

Rather than using a B-mode ultrasound, with typical frequencies in the range of 3–7 MHz, we employ a circular array of twenty-two 0.5 MHz transducers that can be mounted as a collar on a clinical lithotripter. Using a lower frequency allows us to minimise the attenuation of the signal as it propagates through several layers of tissue. The aim of this work is to localise kidney stones in real-time, in order to provide a trigger signal for a lithotripter when the stone is in the focal region. Each transducer, in turn, transmits a short, low-pressure pulse. All the transducers record the backscatter from the stone. The arrival time of the echo on each recording is determined using threshold detection, and then a trilateration algorithm is used to determine the stone location. The elements are placed on the edge of the lithotripter aperture, to yield a larger aperture compared to B-mode. In this paper, we show an assessment of the accuracy of our system to locate targets. Furthermore, the real-time performance of the algorithm is demonstrated.

^{a)}Electronic mail: robin.cleveland@eng.ox.ac.uk

II. METHODS

A. Trilateration algorithm

Figure 1 shows the configuration of the system: an array of N transducers placed at locations \vec{x}_k^T , where \vec{x} refers to a three dimensional vector in space and k is an integer from 1 to N . Pulses are transmitted by transducer k , scatter off the stone located at \vec{x}^S , and received by transducer m . The total distance travelled by sound for any combination of transducers is given by

$$x_{km} = |\vec{x}^S - \vec{x}_k^T| + |\vec{x}_m^T - \vec{x}^S|. \quad (1)$$

It follows that the echo time, t_{km} , in a medium of uniform sound speed, c_0 , between transmitting by transducer k and reception by transducer m is

$$t_{km} = \frac{x_{km}}{c_0}. \quad (2)$$

By using multiple transducers, the location of the stone, \vec{x}^S , can be determined algebraically using Eq. (2). In principle, three measured echo times are sufficient if the speed of sound in the medium and the locations of the transducers are known. In practice however, the echo time for each transmitter-receiver combination may differ from the ideal case due to a number of factors, including the irregular shape of the stone, a non-uniform speed of sound, noise in the signal, uncertainty in the exact location of each element in the array, and the finite size of the transducers and the scatterer. Therefore, the approach here is to take many more measurements from which the error function, e_{km} , is defined,

$$e_{km} = |c_0 t_{km} - \hat{x}_{km}|, \quad (3)$$

where \hat{x}_{km} is the estimated distance travelled by sound, and estimate the stone location by minimising the mean square error

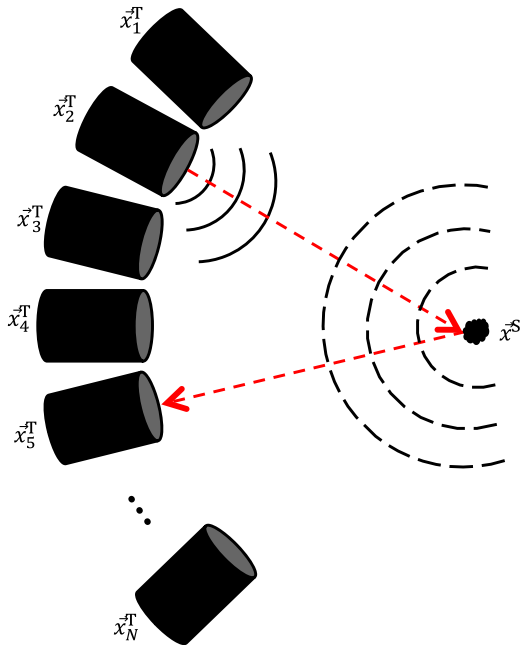


FIG. 1. (Color online) Schematic drawing of an array with N transducers and a scatterer illustrating the sound path between any two transducers.

$$\bar{E} = \frac{1}{N^2} \sum_{m=1}^N \sum_{k=1}^N e_{km}^2. \quad (4)$$

B. Experimental setup

Figure 2 shows the experimental setup consisting of a circular array of transducers and a scatterer. Twenty-two transducers (0.5 MHz, 19.05 mm diameter, V318-SU Panametrics-NDT, Waltham, MA) were placed in a 3D printed collar on a circle of diameter 206 mm. The axis of each transducer was aligned to a point 128 mm away in the z -direction; this corresponds to the focal length of a clinical lithotripter; the Dornier HM3.²¹ The Rayleigh distance for each transducer at 0.5 MHz is 95 mm, and therefore, the lithotripter focus, where the stone should be, is in the spherical spreading region of the transducers. The -6 dB beam width is 9.2° at 0.5 MHz, which corresponds to a lateral distance of 20.6 mm at the transducer lithotripter focus, which estimates the region stone motion can be detected.

A Verasonics Vantage ultrasound engine (Verasonics Inc, Kirkland, WA) was used to control the transmit-receive sequence, acquire the echo data, and compute the location of stones in real time. Each element was excited with a pulse of amplitude of 50 V and a frequency of 0.5 MHz for two cycles. The echo signal was received on all channels at a sampling rate of 2 MHz, four times the transmit frequency, and processed without filtering or time gain compensation.

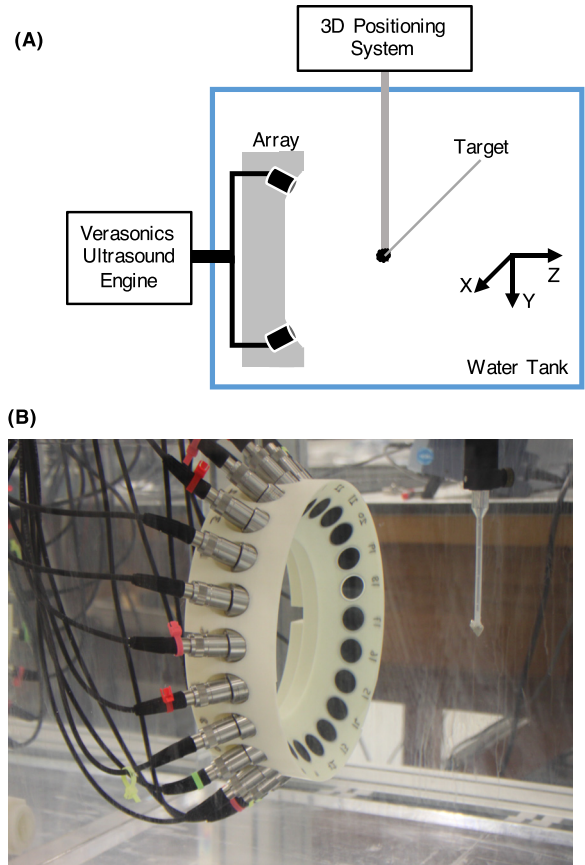


FIG. 2. (Color online) (A) Schematic drawing of the experimental setup. (B) Photograph of the system deployed in a water tank.

Three scatterers were used: two stone models measuring approximately 10 mm by 5 mm by 5 mm cast from UltraCal 30 gypsum cement (United States Gypsum Co., Chicago, IL) and a stone model fragment. The gypsum stones have properties similar to those of natural stones²² and were cast in moulds of natural kidney stones created from micro CT data. The scatterers were glued to the end of a plastic pipette, which was mounted onto a three dimensional positioning stage, so that the stone could be translated under computer control with an accuracy better than 0.1 mm. Subsequently, one of the two stones was fragmented using a lithotripter and the accuracy of the localisation was confirmed for a stone fragment measuring 5 mm by 5 mm by 3 mm.

C. Threshold detection

The measured echo time t_{km} was determined by doing threshold detection on the received signals. Cross-correlation and a combination of detecting the maximum amplitude within a specific time window were tried as an alternative method but were found to be less robust than threshold detection. Four representative raw receive voltage signals for a stone target are shown in Fig. 3. The theoretical arrival time for the cases shown in (A), (B), and (D) is 198 μs and for the case in (C) is 221 μs . It can be seen that the amplitude of the echo varies from 452 to 11 mV, and thus, an absolute threshold would not be appropriate. A study was conducted where the threshold was varied from 3 times to 30 times the standard deviation and it was found that a value of 15 gave the most robust detection. Based on

this criteria, the threshold was approximately 30 mV in (A), (C), and (D), and 47 mV in (B).

In Fig. 3(A), an echo signal is detected at 197 μs , which compares well with the expected arrival of 198 μs , with reverberations within the stone resulting in about 20 μs of secondary signals. In Fig. 3(B), the echo is composed of multiple echoes of varying amplitude. As a result, the threshold employed here results in an arrival time of 193 μs ; about 6 μs after the initial increase in the amplitude beyond noise, a little earlier than expected. Figure 3(C) shows an example, where the directly incident transmitted pulse is recorded on the receiver after 94 μs , while the echo from the stone is received at 217 μs . To avoid detecting the incident signal as an echo, it was assumed that the target will not move beyond ± 20 mm from the focus in any direction in which case the echo from the stone would only be received from 151 to 244 μs . Within ± 20 mm of the focus, the directivity of the pressure field is uniform to $\pm 30\%$, and thus, the amplitude of the scattered signal should also be relatively uniform in that region. Figure 3(D) illustrates a situation where no scatterer could be identified by the threshold algorithm as the noise characterisation resulted in a threshold of 29 mV, which exceeded the 11 mV amplitude of the echo. Decreasing the threshold to five times the standard deviation would have meant this particular signal was detected but would have led to false detection elsewhere.

By using 22 transducers in the array, up to $22^2 = 484$ signals for each localisation are recorded. Therefore, even if individual stone echo signals do not produce a detectable signal, there should be sufficient redundancy to have a robust estimate of the stone location. An assessment of how many transducers are necessary for an accurate localisation will be presented later.

D. Error minimisation behaviour

The error function given in Eq. (4) was minimised with the MATLAB function *fminsearch*, which uses the simplex search method.²³ Figures 4(A) and 4(B) show the error as a function of iteration number and the estimated stone location for a stone placed at the focus. It can be seen that the mean square error steadily decreases and converges to a function output of 4.3×10^{-5} within 47 iterations (using an initial guess, \vec{x}_0 , as the geometric focus). In space, the z coordinate and the radial distance monotonically approach asymptotic values and the final estimate for the position is within 1.3 mm of the true position.

Figures 4(C) and 4(D) show equivalent results for a stone 21.2 mm away from the initial guess. The search algorithm appears to settle around a local minimum for 20 iterations revealed by the flat portion of the error function. In the first few iterations, the z coordinate settles close to the true location -15 mm, as shown in panel (D). Then the algorithm adjusts the radial distance with the final location reached after 86 iterations yielding an error value of 6.7×10^{-5} . This location is 0.4, 3.1, and 0.1 mm away from the true location in x , y , and z , respectively.

The iterative minimisation algorithm was terminated, when the last steps of all coordinates of the estimated location were smaller than 0.1 mm and the change in the mean

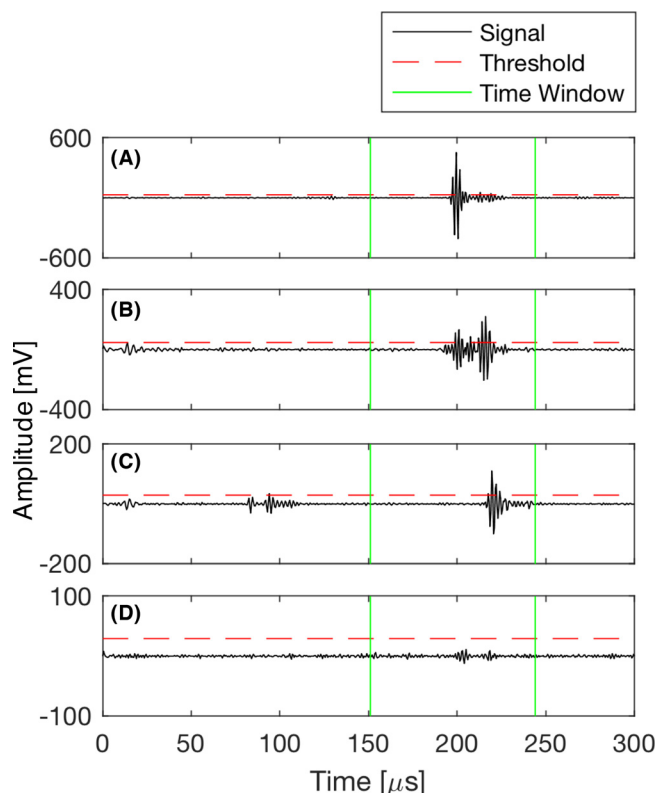


FIG. 3. (Color online) Representative receive signal traces highlighting the threshold detection for a stone target. The theoretical arrival time in (A), (B), and (D) is 198 μs and in (C) is 221 μs .

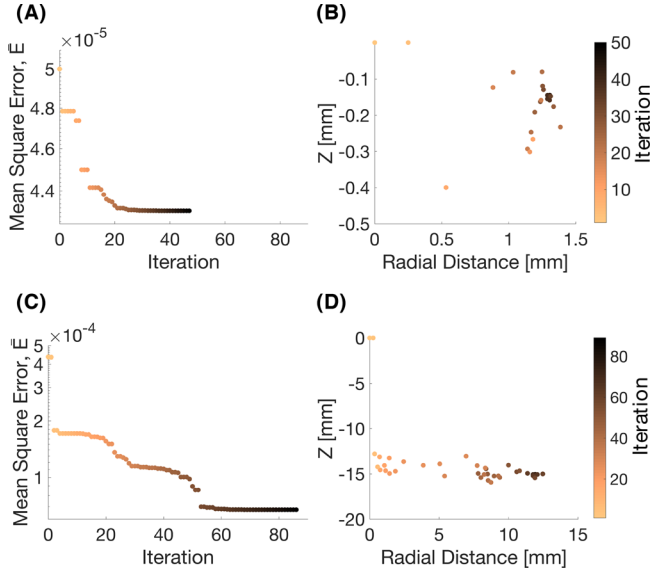


FIG. 4. (Color online) Minimization algorithm: (A) and (B) stone placed at the focus (0, 0, 0), where (A) shows the error function at each iteration and (B) shows the computed target location at each iteration with the final computed location (−0.1, 1.3, 0.1). (C) and (D) stone placed 21 mm away from the focus (0, 15, −15), the final computed location (0.4, 11.9, −15.1).

square error was smaller than 10^{-10} . These values were chosen such that the algorithm does not get stuck in local minima and resulted in a computational time of 25 ms on average for an \bar{x}_0^S within ± 10 mm of the actual location.

It was found that varying $\bar{x}_0^S \pm 25$ mm away from the focus in any direction had a minor effect on the final estimate (less than 0.1 mm) but the computational time was reduced when the initial guess was close to the actual location. Therefore, in the motion experiments, the initial guess was set to the previous location obtained.

Once the optimisation had been run, it was observed that some echo times, $t_{k,m}$, were significantly different from what would be expected from the initial result. Hence, prior to running the minimisation algorithm, the mean echo time and the standard deviation within the dataset were determined. Any echo times that were different by more than 1 standard deviation were excluded to avoid including echoes from structures other than the stone in the minimisation. The proportion of excluded echoes defined as

Excluded echoes %

$$= \frac{\text{No. of echo times within 1 STD}}{\text{Total No. of signals}} \times 100\% \quad (5)$$

turned out to be a predictor of the accuracy of the localization.

III. RESULTS

A. Localisation accuracy

The accuracy of localising targets was determined by moving a stone in the focal region and comparing the true location to that estimated by the tracking algorithm. Figure 5 shows the RMS deviation in location in both lateral directions and along the axis of the lithotripter for two intact gypsum stones and one gypsum stone fragment for locations in a range up to 15 mm from the focus. The RMS deviation is used to measure the difference between estimated coordinates, \hat{x} , \hat{y} , and \hat{z} , and the true values x_t , y_t , and z_t ,

$$\text{RMS dev.} = \sqrt{\frac{(x_t - \hat{x})^2 + (y_t - \hat{y})^2 + (z_t - \hat{z})^2}{3}}. \quad (6)$$

Figures 5(A) and 5(B) show for lateral motion the deviation less than 2 mm for ranges up to 10 mm from the focus and in the axial direction the deviation was less than 2 mm for all ranges tested.

Figure 6 shows the accuracy in orthogonal two-dimensional planes for all three targets. In the lateral plane (upper images), it can be seen that the error within the square spanning ± 5 mm from the focus yields errors less than 3 mm. In the axial plane (lower images), the error is less than 2.5 mm for ranges of ± 15 mm in the axial direction and ± 5 mm in the lateral direction.

B. Uncertainty estimation

The data in Figs. 5 and 6 show that as the target moves away from the focus the localisation accuracy reduces. Two metrics were studied to see if the localised accuracy could be determined from the echo data. One metric was the mean square error, \bar{E} , given in Eq. (4), which was hypothesised to

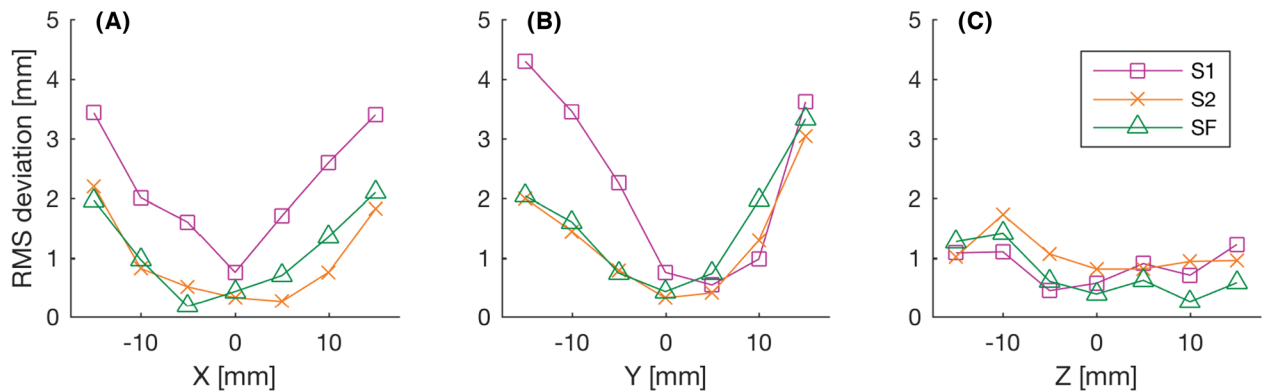


FIG. 5. (Color online) RMS deviation of the localisations for two stone models (S1/S2) and a stone fragment (SF) along the transverse directions [(A) and (B)] and the axial direction (C). In each of the cases the other variables are kept at the focal plane, i.e., for panel (A): $y = z = 0$.

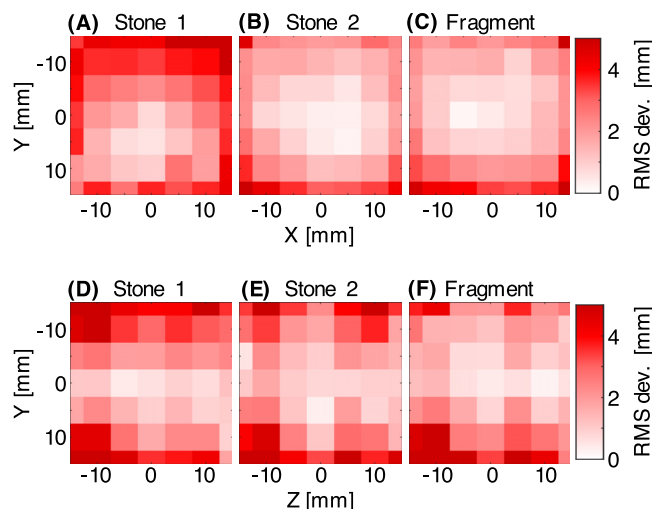


FIG. 6. (Color online) RMS deviation of the localisations for the three different targets (A)–(C) in the lateral and (D)–(F) axial planes.

be small when the accuracy was highest; the second was the number of echo signals within one standard deviation of the mean of the echo times in the dataset, defined as the excluded echoes in Eq. (5).

Figure 7(A) shows the mean square error, \bar{E} , as a function of the deviation for targets placed ± 30 mm from the focus and Fig. 7(B) shows the percentage of excluded echoes as a function of the RMS deviation. In Fig. 7(A), it can be seen that there is a poor correlation between the mean square error and the deviation. In Fig. 7(B), however, it can be seen that the excluded echoes resemble a receiver operator curve. With the exception of one point, localisations that were made with fewer than 60% excluded echoes yield a deviation of less than 5 mm. With the exception of nine further points, any localisation that was computed with fewer than 80% excluded echoes also results in less than 5 mm deviation. These nine points all stem from targets placed 20 to 30 mm away from the focus in the lateral direction, which is beyond the region of a uniform pressure field of the transducers.

Using the data in Fig. 7(B) a threshold can be defined to determine if a SW should be fired to break up stones detected to be in the focal zone or not. A threshold of 60% excluded echoes yielded a 4.9% false-positive rate (that is, deviation was >4 mm but not rejected) and a 34.9% detect rate (that is, localisations of better than 4 mm was identified). By applying an excluded echoes percentage threshold of 80% these rates will change to 19.5% and 72.3%, respectively.

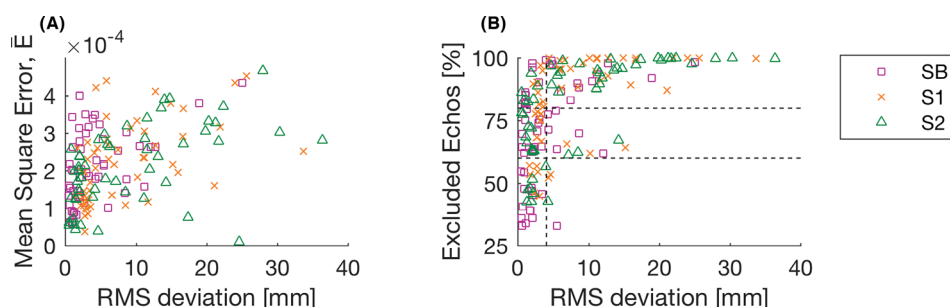


FIG. 7. (Color online) Comparing the mean square error (A) and the percentage of excluded echoes (B) to the true deviation to determine a metric for an uncertainty estimate.

C. Number of transducers

The collar was fabricated for 22 transducers, however, it may be possible to achieve sufficient results with fewer transducers, which would reduce acquisition and processing times. The impact of using fewer transducers was accomplished by post-processing full data sets and only using a subset of transducers. The transducers were chosen such that the aperture was not changed and such that active elements were always equally spaced. Figure 8 shows the error along all three directions for 3, 6, 11, and 22 transducers. It can be seen that 11 and 22 transducers result in an almost identical error profile. Using six transducers results in a similar profile for all but two off-axis locations. Finally, using three transducers the stone cannot be located reliably in the lateral directions nor on-axis. The accuracy is worse than 5 mm in two locations.

The processing time was 25 ms for 22 elements, 10 ms for 11 elements, 5.8 ms for 6 elements, and 4.3 ms for 3 elements.

D. Moving targets

Figure 9 shows the results of localising a stone that was in continuous motion (range ± 10 mm) across the focus in the lateral direction using 22 elements. The colour coding of each localisation identifies the uncertainty (percentage of excluded echoes) in the localisation. The location is estimated accurately when the stone is within ± 7.5 mm of the focus and the uncertainty is low. When the stone moves to ± 10 mm, the localisation has an error of <7.5 mm, however, the uncertainty is also high, which means the information can still be used for gating. Note however, the previously identified excluded echoes threshold for stones (60% to 80%) is different in these data where even up to a value of 86% excluded echoes the localisations are accurate.

IV. DISCUSSION

It has been shown that a trilateration approach, combined with a minimisation algorithm, can be used to localise kidney stones *in vitro*. The results reported here show (for all tested scatterers) that, with the exception of one point, the accuracy is better than 3 mm for stones within ± 10 mm of the focus in the lateral direction. Localisations became significantly less accurate at lateral distances greater than ± 10 mm from the focus, which was expected, given the beam width of the transducers. We note that the focal width of current lithotripters ranges from 2.8 to 7.7 mm,²⁴ and

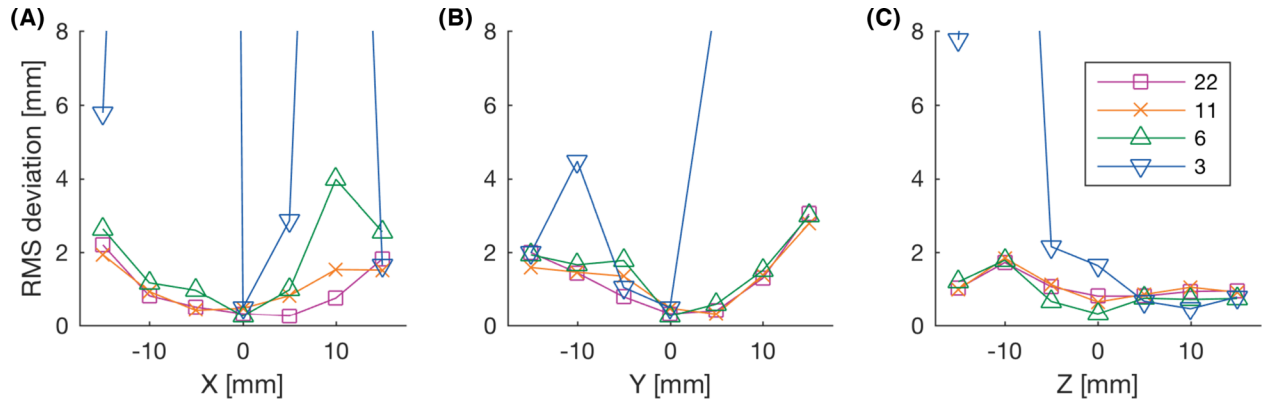


FIG. 8. (Color online) RMS deviation of the localisations for a stone model, using 3, 6, 11, or 22 transducers from the collar, in the transverse directions [(A) and (B)] and the axial direction (C).

therefore, correctly identifying whether the stone is in the focal volume within ± 10 mm is sufficient to gate SWs for the application at hand.

A correlation between the accuracy of the localisation and the number of transducers that pick up an echo time within 1 standard deviation of the mean echo time in that dataset, the percentage of excluded echoes as defined in Eq. (5), was determined. This metric was more robust as a predictor of uncertainty than the mean square error, \bar{E} . Analysing the current datasets suggests a threshold between 60% and 80% of excluded echoes can be used to determine if the stone localisation is accurate. For more complex media such as tissue, we anticipate that the variation in this threshold could be even greater. It may be that the threshold detection for an accurate localisation must be determined for each patient, a process that could be achieved by taking an initial measurement when the stone is in a known location. Fluoroscopy is typically used for alignment at the start of lithotripsy and an initial ultrasound measurement when the stone is in the focus could be used to estimate an appropriate threshold of Excluded Echoes for robust localisations.

Furthermore, lithotripters that differ in focal width might require different thresholds from 60% or 80% that were optimised for an acceptable deviation of <4 mm. Table I shows how the detection rates (DR) and the false positive rates (FP) change for acceptable RMS deviations [defined in

Eq. (6)] of <2 mm, <4 mm, and <8 mm, and for 60% and 80% Excluded Echoes. Here, the compromise lies in reducing treatment times while minimising the risk of missing the target. For lithotripters with larger focal widths (and thus a higher acceptable deviation), it might be appropriate to set a higher threshold to reduce treatment times. It can be seen that an acceptable deviation of <8 mm yields a FP of 12% for 80% excluded echoes. This value is similar to the FP of 13% for a deviation of <2 mm and 60% excluded echoes. The higher DR at a higher excluded echoes threshold of 80% would result in a faster treatment time and might thus be desirable. Lithotripters with narrower foci, however, require a lower threshold in order to decrease FP rates.

It was shown that decreasing the number of transducers reduces the acquisition time but also results in poorer performance. For three elements it was not possible to robustly locate the stone. It should be noted that in tissue, signals will be subject to a greater degree of non-ideal behaviour, and so, although it was sufficient *in vitro*, it would not be a surprise if all 22 (maybe even more) transducers would be needed in tissue.

Using a MATLAB code, it was possible to acquire and process data in approximately 1 s using 22 elements. Given lithotripters fire rates are on the order of 1 to 2 Hz, this is not quite sufficient. Implementing the algorithm in a compiled code should reduce the time dramatically, it is noted that the acquisition time for recording $300 \mu\text{s}$ on 22 transducers is 6.6 ms, and so, for processing times of <0.1 s, real-time stone tracking can be carried out.

The scope of the experiments up to this stage have been mainly limited by two factors. First, all experiments have

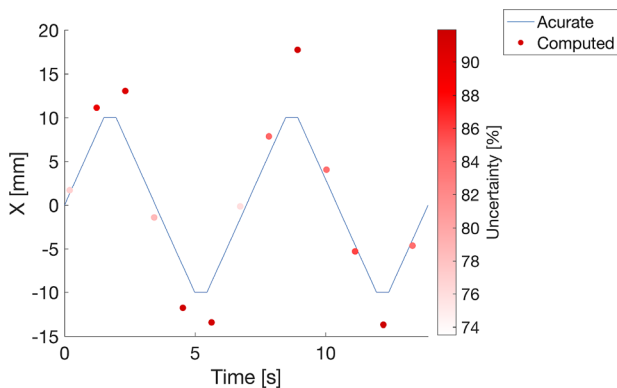


FIG. 9. (Color online) Localising a moving stone that is displaced ± 10 mm from the focus and showing its true location as a line and the estimates as red points. The colourbar identifies the percentage of excluded echoes to predict the accuracy of each localisation.

TABLE I. Detection rates (DR) (better than acceptable deviation and correctly identified) and false positive rates (FP) (above acceptable deviation but not rejected) for 60% and 80% excluded echoes for different acceptable RMS deviations.

Excluded echoes threshold Accepted RMS deviation	60%		80%	
	DR	FP	DR	FP
< 2 mm	44%	13%	79%	36%
< 4 mm	35%	4.9%	72%	20%
< 8 mm	29%	0%	62%	12%

been conducted in water, a homogeneous medium with low attenuation and known sound speed. In tissue, the signals would be subject to scattering and reflections from different tissue interfaces (e.g., fat and muscle), and the signals would be weaker due to higher absorption. In these complex structures, weighting different echo times based on the robustness of the echo, the amplitude of the signal, or the noise level might be advantageous. In the homogeneous environment, however, applying weights has not resulted in an improved accuracy. Second, for the current experiments only one scatterer has been placed in the acoustic field. During SWL, however, stones will break into multiple fragments and multiple stone fragments will be present in the field. It would be necessary to show the system remains robust in the presence of multiple fragments.

V. CONCLUSIONS

In summary, it has been shown that for a low-element count array in a configuration appropriate for a lithotripter it is possible to track a model kidney stone with an accuracy better than 4 mm near the focus. This system could be used to gate SW delivery in order to reduce SWs that are not targeted on the stone. Furthermore, it would indicate if motion had moved the stone permanently out of the focus. The proposed system would not interfere with other imaging modalities such as X-ray fluoroscopy or B-mode ultrasound. The approach measured echo times between multiple transducers using a threshold detection to determine the echo time. A minimisation approach was employed to determine the most likely position of the stone. An uncertainty parameter has been identified that can be used to exclude inaccurate results. Finally, the method can be used to track moving targets in real time. Accessing the robustness of the method in more realistic complex tissue structures is now necessary.

ACKNOWLEDGMENTS

We would like to thank Dr. Jonathan Kracht for the initial design of the circular array of transducers and Dr. Erasima Lyka and Dr. Christian Coviello for their help on working with the Verasonics. This work has been supported in part by the NIH through Grant No. P01-DK43881. The raw data are available through the Oxford University Research Archive (ORA).

- ¹C. Chaussy, W. Brendel, and E. Schmiedt, "Extracorporeally induced destruction of kidney stones by shock waves," *Lancet* **316**(8207), 1265–1268 (1980).
- ²P. M. Knapp, T. B. Kulb, J. E. Lingeman, D. M. Newman, J. H. Mertz, P. G. Mosbaugh, and R. E. Steele, "Extracorporeal shock wave lithotripsy-induced perirenal hematomas," *J. Urol.* **139**(4), 700–703 (1988).
- ³J. V. Kaude, C. M. Williams, M. R. Millner, K. N. Scott, and B. Finlayson, "Renal morphology and function immediately after extracorporeal shock-wave lithotripsy," *Am. J. Roentgenol.* **145**(2), 305–313 (1985).
- ⁴J. A. McAteer and A. P. Evan, "The acute and long-term adverse effects of shock wave lithotripsy," *Semin. Nephrol.* **28**, 200–213 (2008).
- ⁵A. K. Tuteja, J. P. Pulliam, T. H. Lehman, and L. W. Elzinga, "Anuric renal failure from massive bilateral renal hematoma following extracorporeal shock wave lithotripsy," *Urology* **50**(4), 606–608 (1997).

- ⁶B. Lipski, J. Miller, G. Rigaud, G. Stack, and C. Marsh, "Acute renal failure from a subcapsular hematoma in a solitary kidney: An unusual complication of extracorporeal shock wave lithotripsy," *J. Urol.* **157**(6), 2245 (1997).
- ⁷G. Janetschek, F. Frauscher, R. Knapp, G. Hofle, R. Peschel, and G. Bartsch, "New onset hypertension after extracorporeal shock wave lithotripsy: Age related incidence and prediction by intrarenal resistive index," *J. Urol.* **158**(2), 346–351 (1997).
- ⁸N. Mandel, I. Mandel, K. Fryjoff, T. Rejniak, and G. Mandel, "Conversion of calcium oxalate to calcium phosphate with recurrent stone episodes," *J. Urol.* **169**(6), 2026–2029 (2003).
- ⁹R. Newman, R. Hackett, D. Senior, K. Brock, J. Feldman, J. Sosnowski, and B. Finlayson, "Pathologic effects of ESWL on canine renal tissue," *Urology* **29**(2), 194–200 (1987).
- ¹⁰R. Thomas, J. Roberts, B. Sloane, and B. Kaack, "Effect of extracorporeal shock wave lithotripsy on renal function," *J. Endourol.* **2**(2), 141–144 (1988).
- ¹¹L. R. Willis, A. P. Evan, B. A. Connors, Y. Shao, P. M. Blomgren, J. H. Pratt, N. S. Fineberg, and J. E. Lingeman, "Shockwave lithotripsy: Dose-related effects on renal structure, hemodynamics, and tubular function," *J. Endourol.* **19**(1), 90–101 (2005).
- ¹²M. Delius, M. Jordan, H. Eizenhoefer, E. Marlinghaus, G. Heine, H.-G. Liebich, and W. Brendel, "Biological effects of shock waves: Kidney haemorrhage by shock waves in dogs administration rate dependence," *Ultrasound Med. Biol.* **14**(8), 689–694 (1988).
- ¹³A. P. Evan, J. A. McAteer, B. A. Connors, P. M. Blomgren, and J. E. Lingeman, "Renal injury during shock wave lithotripsy is significantly reduced by slowing the rate of shock wave delivery," *Br. J. Urol.* **100**(3), 624–628 (2007).
- ¹⁴B. A. Connors, A. P. Evan, L. R. Willis, P. M. Blomgren, J. E. Lingeman, and N. S. Fineberg, "The effect of discharge voltage on renal injury and impairment caused by lithotripsy in the pig," *J. Am. Soc. Nephrol.* **11**(2), 310–318 (2000).
- ¹⁵R. O. Cleveland, R. Anglade, and R. K. Babayan, "Effect of stone motion on *in vitro* comminution efficiency of Storz Modulith SLX," *J. Endourol.* **18**(7), 629–633 (2004).
- ¹⁶M. Orkisz, T. Farchtchian, D. Saighi, M. Bourlion, N. Thiounn, G. Gimenez, B. Debre, and T. A. Flam, "Image based renal stone tracking to improve efficacy in extracorporeal lithotripsy," *J. Urol.* **160**(4), 1237–1240 (1998).
- ¹⁷M. Orkisz, M. Bourlion, G. Gimenez, and T. A. Flam, "Real-time target tracking applied to improve fragmentation of renal stones in extracorporeal lithotripsy," *Mach. Vis. Appl.* **11**(3), 138–144 (1999).
- ¹⁸C. C. Chang, S. M. Liang, Y. R. Pu, C. H. Chen, I. Chen, T. S. Chen, C.-L. Kuo, F. M. Yu, and Z. F. Chu, "In vitro study of ultrasound based real-time tracking of renal stones for shock wave lithotripsy: Part I," *J. Urol.* **166**(1), 28–32 (2001).
- ¹⁹C. C. Chang, I. Manousakas, Y. R. Pu, S. M. Liang, C. H. Chen, T. S. Chen, F. M. Yu, W.-H. Yang, Y.-C. Tong, and C.-L. Kuo, "In vitro study of ultrasound based real-time tracking for renal stones in shock wave lithotripsy: Part II—A simulated animal experiment," *J. Urol.* **167**(6), 2594–2597 (2002).
- ²⁰M. D. Sorensen, J. D. Harper, R. S. Hsi, A. R. Shah, M. K. Dighe, S. J. Carter, M. Moshiri, M. Paun, W. Lu, and M. R. Bailey, "B-mode ultrasound versus color Doppler twinkling artifact in detecting kidney stones," *J. Endourol.* **27**(2), 149–153 (2013).
- ²¹M. A. Averkiou and R. O. Cleveland, "Modeling of an electrohydraulic lithotripter with the KZK equation," *J. Acoust. Soc. Am.* **106**(1), 102–112 (1999).
- ²²J. A. McAteer, J. C. Williams, Jr., R. O. Cleveland, J. Van Cauwelaert, M. R. Bailey, D. A. Lifshitz, and A. P. Evan, "Ultrasound gypsum artificial stones for research on the mechanisms of stone breakage in shock wave lithotripsy," *Urol. Res.* **33**(6), 429–434 (2005).
- ²³J. C. Lagarias, J. A. Reeds, M. H. Wright, and P. E. Wright, "Convergence properties of the Nelder–Mead simplex method in low dimensions," *SIAM J. Optim.* **9**(1), 112–147 (1998).
- ²⁴R. O. Cleveland and J. A. McAteer, "The physics of shock wave lithotripsy," in *Smith's Textbook of Endourology*, 3rd ed., edited by Arthur D. Smith, G. Preminger, G. Badlani, and L. R. Kavoussi (Wiley-Blackwell, Hoboken, NJ, 2012), Vols. 1 and 2, pp. 527–558.